Published in final edited form as:
Proteins. 2010 October ; 78(13): 2798–2808. doi:10.1002/prot.22794.

Fold versus Sequence Effects on the Driving Force for Protein Mediated Electron Transfer

Bradley Scott Perrin Jr. and **Toshiko Ichiye***
Department of Chemistry, Georgetown University, Box 571227, Washington, DC 20057-1227

Abstract

Electron transport chains composed of electron transfer reactions mainly between proteins provide fast, efficient flow of energy in a variety of metabolic pathways. Reduction potentials are essential characteristics of the proteins because they determine the driving forces for the electron transfers. Since both polar and charged groups from the backbone and side chains define the electrostatic environment, both the fold and the sequence will contribute. However, while the role of a specific sequence may be determined by experimental mutagenesis studies of reduction potentials, understanding the role of the fold by experiment is much more difficult. Here, continuum electrostatics and density functional theory calculations are used to analyze reduction potentials in [4Fe-4S] proteins. A key feature is that multiple homologous proteins in three different folds are compared: six high potential iron-sulfur proteins, four bacterial ferredoxins, and four nitrogenase iron proteins. Calculated absolute reduction potentials are shown to be in quantitative agreement with electrochemical reduction potentials. Calculations further demonstrate that the contribution of the backbone is larger than that of the side chains and is consistent for homologous proteins but differs for non-homologous proteins, indicating that the fold is the major protein factor determining the reduction potential while the specific amino acid sequence tunes the reduction potential for a given fold. Moreover, the fold contribution is determined mainly by the proximity of the redox site to the protein surface and the orientation of the dipoles of backbone near the redox site.

Introduction

Metalloproteins are found throughout living organisms and perform a variety of different functions, most commonly as electron carriers for such important biological processes as respiration, photosynthesis, and nitrogen fixation.1 Biological electron transport entails moving electrons quickly and efficiently over distances of 10 to 30 Å by a process in which electrons hop between redox sites,2،3 which include iron-sulfur clusters, hemes, and chlorophylls. Protein-mediated electron-transfer offers several evolutionary advantages over small-molecule mediated transfer. For instance, the protein may serve as a scaffold to hold the redox site at a desired location, such as in the membrane, or provide a recognition site for an electron donor or acceptor. In addition, the protein can alter the electron transfer properties of the redox site by providing a well-defined electrostatic environment for the redox site that differs from aqueous environment of the cell. Specifically, the electrostatic potential created by the protein can change the redox site's reduction potential, which determines the driving force for an electron transfer reaction, to a value optimal for a specific electron transfer. Moreover, since the reduction potential is a direct probe of the local electrostatic potential at the redox site, studies of reduction potentials are important for

*To whom correspondence should be addressed. Phone: 202-687-3724, FAX: 202-687-9620, ti9@georgetown.edu.

understanding the underlying molecular basis of electrostatic environments in proteins, such as the active site of an enzyme on its activity.

Because the protein environment around the redox site is defined by the three-dimensional structure of the polypeptide chain, the question arises as to the relative contributions of the fold versus the sequence to the reduction potential of a protein. It is well known that similar folds generally indicate similar functions while the specific sequence can tune the function. However, it is less obvious that similar folds of metalloproteins indicate similar redox properties while the specific sequence can tune the redox properties.[4,5] In fact, an early proposal was that the reduction potential of a protein was controlled by its net charge.[6] Consequences are that single mutations will rarely destroy functionality by causing large changes in reduction potential since the overall fold is generally robust with respect to mutations but also that single mutations may tune the reduction potential to optimize a given electron transfer chain by causing small changes in the reduction potentials.

The preponderance of homologous proteins with the same redox site that have vastly different sequences and yet similar electrochemical reduction potentials support the idea that the fold must be a major contributor. However, quantifying the contribution of the fold to reduction potentials by experiment is difficult and mostly indirect. Thus, calculations provide an important means of examining the different contributions to the electrochemical potential. For the reduction reaction $A + e^- \rightarrow A^-$, the reduction potential $E°$ is related to the reaction free energy $\Delta G°$ by

$$-nFE^\circ = \Delta G^\circ \approx \Delta G_{\text{in}} + \Delta G_{\text{out}} + \Delta G_{\text{SHE}} \quad (1)$$

where n is the number of electrons and F is Faraday's constant.[7] Furthermore, $\Delta G°$ can be approximately decomposed into ΔG_{in}, the inner sphere or intrinsic energy required to add an electron to the redox site, ΔG_{out}, the outer sphere or change upon reduction in the interaction energy of the redox site with its environment, and $\Delta G_{\text{SHE}} = 4.43$ eV, the free energy for the electron in the standard hydrogen electrode.[8] ΔG_{in} is determined primarily by the type of redox site and can be obtained from quantum chemical calculations of the redox site in both oxidation states. On the other hand, ΔG_{out} is determined mainly by the electrostatic environment created by the protein and surrounding solvent and can be obtained from classical electrostatic calculations of the system in both oxidation states.

The iron-sulfur proteins, which are ubiquitous and play numerous roles in essential biological processes, are ideal for addressing the role of fold versus sequence. Fe-S proteins most commonly contain $[Fe(SR)_4]$, $[Fe_2S_2(SR)_4]$, $[Fe_4S_4(SR)_4]$, or $[Fe_3S_4(SR)_4]$ clusters, and the same cluster can be found in many different folds. The synthetic clusters of Holm and co-workers[9] enable comparisons of a redox site cluster in a protein with the same cluster in solution, thus probing the advantages of protein mediated versus small-molecule mediated electron transfer. The small water soluble Fe-S proteins from bacteria are idea for calculations and mutational studies. Moreover, small Fe-S proteins have been proposed as primordial electron carriers[10,11] and thus may help define the essential features of protein-mediated transfer.

A classic problem in the Fe-S proteins is the origin of the vastly different reduction potentials of the high-potential iron-sulfur proteins (HiPIPs) versus the [4Fe-4S]-ferredoxins (Fds), which both contain the $[Fe_4S_4(S\text{-}Cys)_4]$ cluster, but under physiological conditions only the 1-/2- couple is accessible to the HiPIPs and only the 2-/3- couple is accessible to the Fds. In addition, the iron protein (FeP) from nitrogenase has a $[Fe_4S_4(S\text{-}Cys)_4]$ cluster that can access the 2-/3- and apparently even the 3-/4- couples under physiological conditions.[12]

HiPIP and Fd are similar in size, while FeP is significantly larger and all three have very different folds (Fig. 1). The stabilization of different couples between the HiPIPs and Fds has been attributed to the backbone and solvent dipoles by calculations5,13,14 and experiment,15 although the relative importance of hydrogen bonding versus simple polar interactions is still not clear. Specifically, based on calculations of three ferredoxins and one HiPIP, Warshel has proposed that the backbone is a major differentiating factor between the different folds, while the solvent dipoles differentiate the ferredoxins.14,16 Additionally, when the folds are identical, sequence determinants have bee identified that cause shifts in reduction potentials of 50 to 100 mV in the rubredoxins17,18 and ferredoxins19 as well as bound water molecules that also play key roles in the rubredoxins20–22 and in ferredoxins23,24. However, differences in the electronic structure of the cluster in the HiPIPs versus the Fds25,26 and electronic perturbation of the cluster by water15 have also been attributed to cause part of the difference, although perturbations due to hydrogen bonds are apparently small27 and the dihedral angles of the ligands appear to be more important28. Thus, while the major role of the backbone and thus the fold in the reduction potential has been discussed4,5, unraveling the importance of the cluster, fold, and sequence by calculation have been hindered because of the difficulty in separating electronic versus protein effects. Moreover, systematic studies of multiple homologs have not been performed to establish the consistency of the fold contribution.

Here, the nature of the protein environmental contribution is examined in high-resolution crystal structures of six HiPIPs, four Fds, and two FePs plus an ADP-bound FeP and a FeP homolog (all four will be referred to as FeP proteins), looking for consistencies within a fold and differences between folds. The intrinsic contributions ΔG_{in} are from broken symmetry density functional theory (BS-DFT) calculations,26,29 which we have calibrated to predict adiabatic and vertical dissociation energies of a variety of Fe-S clusters in the gas phase that are in good agreement with photoelectron spectroscopy.30–33 The environmental contributions ΔG_{out} are calculated using the model developed by Honig and co-workers34,35 in which the Poisson or Poisson-Boltzmann (PB) equation is solved numerically for the protein represented as partial charges in a low dielectric continuum cavity and the surrounding solvent represented as a high dielectric continuum. The use of high-resolution crystal structures rather than molecular dynamics mechanics simulations assures that the structures used for the calculations are not dependent on the force field since our work indicates that the reduction potential is very sensitive to the exact geometry near the cluster.19,36 The two calculations can be performed separately for Fe-S proteins as shown by Noodleman, Case, and co-workers.13 Our calculated ΔG_{in} and ΔG_{out} together with ΔG_{SHE} (Eqn. 1) are shown here to give reduction potentials in excellent agreement with electrochemical measurements. By separating the contributions of the protein cavity and the backbone, which determines the fold effects, and the side chains, which determine the sequence effects, the calculations demonstrate that the protein cavity and backbone contributions are consistent within a given protein fold but differ between folds for the six HiPIPs, four Fds, and four FePs. The calculations also show that the protein fold is the major protein factor determining the reduction potential while the specific amino acid sequence tunes the reduction potential for a given fold. Finally, the calculations show that the protein fold contributes mainly by determining the proximity of the redox site to the protein surface and by defining the number, location, and orientation of the dipoles of backbone within ~10 Å of the redox site center.

Methods

All crystal structures were obtained from the Protein Data Bank (PDB).37 Crystal structures of six HiPIPs were from *Rhodocyclus tenuis* (*Rt*) at 1.50 Å resolution [1ISU]],38 *Rhodoferax fermentans* (*Rf*) at 1.45 Å resolution [1HLQ],39 *Ectothiorhodospira vacuolata*

(*Ev*) at 1.80 Å resolution [1HPI],40 *Ectothiorhodospira halophila* (*Eh*) at 2.50 Å resolution [2HIP],41 *Thermochromatium tepidum* (*Tt*) at 0.80 Å resolution [1IUA],42 and *Chromatium vinosum* (*Cv*) at 1.20 Å resolution [1CKU]43. In addition, crystal structures of four Fds were from *Clostridium acidiurici* (*Ca*) at 0.94 Å resolution [2FDN],44 *Peptostreptococcus asaccharolyticus* (*Pa*) at 2.00 Å resolution [1DUR],45 *Pseudomonas aeruginosa* (*Pr*) at 1.32 Å resolution [2FGO],46 and *Chromatium vinosum* (*Cv*) at 2.10 Å resolution [1BLU].47 Also used were crystal structures of the ADP-free Fe protein from *Azotobacter vinelandii* (*Av*) solved at 2.2 Å resolution [1G5P,2NIP],48–50 the ADP-bound *Av* Fe protein (*Av*-ADP) solved at 2.15 Å resolution [1FP6],48 the ADP-free Fe Protein from *Clostridium pasteuranium* (*Cp*) solved at 1.93 Å resolution [1CP2],49 and the homologous L protein (BchL) from *Rhodobacter sphaeroides* (*Rs*) solved at 1.63 Å [3FWY].51 A crystal structure for $Fe_4S_4(SCH_2CH_3)_4$52 from the Cambridge Structure Database was used for the analog in solution calculations [CCSD code: COZXUK]. For crystal structures containing more than one protein in the asymmetric unit or multiple side chain conformations, the calculated reduction potentials were averaged over all structures with the exception of *Eh* HiPIP because one of its structures contains unusual Fe-S bond lengths and thus was not utilized. In addition, since two structures of *Av* FeP were solved at the same resolution with the same R-factor, their results were also averaged. The experimental reduction potentials in the HiPIPs for $1^-/2^-$42,53,54 and the $2^-/3^-$55 couples, in the Fds for the 1-/2-56 and 2-/3- couples,46,57,58 and the FePs for the 2-/3-59,60 couple were obtained from the literature. The value for the 1-/2- couple of the FePs is assumed based on the value for the 2-/3-.

The ΔG_{in} were obtained from BS-DFT calculations at the B3LYP/6-31G(++)$_S$**//B3LYP/6-31G** level of $Fe_4S_4(SCH_3)_4^{\ 1-/2-/3-}$ with the dihedral angles C-S-Fe-S_i (where S_i is the cluster sulfur on the opposite plane from the iron) of approximately 60° in one plane and −60° in the other plane in vacuum (Niu & Ichiye unpublished results, see also Supplementary Material) using methods described previously30 with the program NWChem.61 At this level, the adiabatic detachment energy (ADE) of the electron calculated for $Fe_4S_4(SCH_2CH_3)_4^{\ 2-}$ without and with zero point energy (ZPE) corrections are 0.191 and 0.243 eV, respectively, compared to the experimental value of 0.29 eV from gas phase photoelectron spectroscopy.32 The ΔG_{in} including corrections for ZPE and entropy and the electrostatic potential charges along with more details on the calculations are given the supplementary material.

The ΔG_{out} were obtained from Poisson continuum electrostatic calculations of the cluster in the protein surrounded by a continuum solvent utilizing APBS,62 a program for solving the Poisson-Boltzmann equation. Although the ionic concentration here is zero, the calculations are referred to as “PB” following common practice. Details for the calculations are given elsewhere63 and are summarized here. The reference system consists of the cluster; i.e., the iron and inorganic sulfurs, and the ligating cysteinyl sulfurs, β-carbons, and β-hydrogens. ΔG_{out} is the difference in solvation energy of *the cluster* between the oxidized and reduced states.

$$\Delta G_{out} = \Delta G_{solv}([Fe_4S_4(SR)_4]^{n-1}) - \Delta G_{solv}([Fe_4S_4(SR)_4]^n) \quad (2)$$

The solvation energy of oxidation state *n* is the difference between the free energy of $[Fe_4S_4(SCH_3)_4]^n$ in the protein plus the surrounding solvent (note the extra hydrogen is considered a link atom with zero charge) and the free energy of $[Fe_4S_4(SCH_3)_4]^n$ in vacuum. Missing atoms were added to the crystal structures and hydrogen positions were optimized using CHARMM. The HiPIPs and Fds were calculated within a 51.2 Å cubic grid and the FePs were calculated with a 76.8 Å cubic grid; a grid spacing of 0.2 Å was used for all calculations. The atomic radii and partial charges (except for the cluster) were from

CHARMM22 parameters;64 the partial charges for the cluster were from the BS-DFT calculations (see supplementary material). The Connolly surface, i.e., the surface outlined by a probe of radius r = 1.4 Å rolling over the van der Waals surfaces of the solute atoms,65 was used for both the protein-water and the protein-redox site boundaries. After assigning dielectric values to each grid point based on the boundaries defined by the Connolly surfaces, the boundaries were smoothed by reassigning the value for each grid point as the average of the original values of the grid point and its eight nearest neighbors.66 In addition, although there is debate over what ε_p signifies and what its value is,67 $\varepsilon_p = 4$ is used here as a standard value that has been used successfully for many proteins to account for reorientational and electronic polarizability.34

The environmental contributions to the reduction potential were separated as follows. The protein cavity was defined by the Connolly molecular surface of the entire protein including the cluster using the experimental structure. The contribution of the cavity ΔG_{cav} was defined as ΔG_{out} for an empty protein cavity in water by setting all the protein partial charges (excluding the cluster) equal to zero with $\varepsilon_p = 1$, and the contribution of the dielectric-filled cavity $\Delta G_{\varepsilon p}$ was defined similarly except $\varepsilon_p = 4$. The contribution of the backbone ΔG_{bb} was defined as ΔG_{out} calculated for only the backbone atom charges in the entire protein cavity filled with $\varepsilon_p = 4$; here, the side chain for each residue, with the exception of proline and FeS-ligated cysteines, was replaced with a hydrogen atom and the atomic partial charges were set to those of glycine. Backbone contributions of each residue were obtained as the difference between ΔG_{bb} and the free energy calculated with the partial charges of that residue equal to zero. Finally, $\Delta G_{bb(in)}$ and $\Delta G_{bb(out)}$ were calculated by setting the partial charges of all residues equal to zero that either did not have or did have, respectively, a backbone atom within a cutoff of a redox site inorganic or cysteinyl sulfur within the entire protein cavity with $\varepsilon_p = 4$.

Results and Discussion

The experimental reduction potentials for the $[Fe_4S_4]$ proteins follow the trend HiPIPs < Fds < FePs for the 1-/2- and 2-/3- couples (Table I). The reduction potential for the 1-/2- couple of the Fds and FePs is presumably so positive that it is not generally accessible by experiment and has been measured as 0.73 V for *Clostridium pasteurianum* Fd.56 Similarly, the reduction potential for the 2-/3- couple of HiPIPs is presumably so negative that it is also not generally accessible and has been measured as −0.91 V for *Rhodopila globiformis* HiPIP.55 The reduction potentials calculated by DFT and PB (Eqn. 1) using the experimental geometries for each protein are in excellent agreement with experimental reduction potentials (Fig. 2a). The effects of the resolution of the crystal structures on the calculated reduction potentials were examined by calculating the deviation of the values calculated from multiple structures in the asymmetric unit or multiple side chain conformations in the deposited structure as well as the deviation of the calculated from the experimental values (Fig. 2b). The deviation of the calculated values from the structures is approximately less than $|\Delta E°| < \sim -0.04 + 0.06R$ eV and the deviation from experiment is approximately less than $|E°_{calc} - E°_{exp}| < \sim -0.04 + 0.09R$ eV, where R is the resolution. Moreover, other calculations indicate that the larger deviation for *Cp* Fd in the non-biological 1-/2- couple is due to preference for a dihedral transition in the 1- state in the gas phase found in the Fd conformation but not the HiPIP conformation that is restrained by the protein; this leads to a more positive value of $-\Delta G_{in}/F$ for the 1-/2- couple of Fd (Niu & Ichiye, unpublished work). We now take advantage of this agreement between the calculated reduction and experimental reduction potentials to examine what gives rise to the differences between the HiPIPs, Fds, and FePs.

Intrinsic versus environmental contribution

Since the focus here is on the environmental contribution ΔG_{out}, the intrinsic contribution ΔG_{in} for a given redox couple was assumed to be identical for all proteins. The DFT calculations indicate that the 2- state is slightly more stable than the 1- state in vacuum since $-\Delta G_{in}/nF$ was 0.26 V for the 1-/2- couple but that further reduction of the cluster was very unfavorable in vacuum since $-\Delta G_{in}/nF$ was −3.48 V for the 2-/3- couple (Table I), respectively. However, our recent studies indicate that differences in the dihedral angles of the cysteinyl ligands for the different folds may alter the intrinsic contribution,28 mainly for the 1-/2- couple of the Fds (unpublished results) so here we focus on the 2-/3- couple where the variation may be less (Table I). Since the contribution of the electron in the electrode also disfavored reduction by $-\Delta G_{SHE}/F$ = 4.43 eV, ΔG_{out} must be a large positive contribution to the electrochemical reduction potential.

The PB results for ΔG_{out} indicate that the environmental contribution due to the protein and surrounding water was similar for proteins with the same fold but differed by 200 to 300 mV between proteins with different folds (Table I). Another factor may be that the cluster is less buried in the Fds than in the HiPIPs5,13 and is even less buried in the FePs. Since the proximity of the cluster to the protein surface determines how close the high-dielectric solvent can come to the cluster, more buried clusters should have a less positive $-\Delta G_{out}/F$.

Fold versus sequence contributions

The fold determines the size and shape of the protein cavity, the location of the cluster in the cavity, and the arrangement of the partial charges of the backbone while the sequence determines the arrangement of the partial charges of the side chains. Thus, the fold contribution should be characteristic of the backbone irrespective of the sequence. However, separating contributions of the backbone and side chains is difficult since the PB model assumes the protein is a set of partial charges in a dielectric continuum, which is difficult to partition. Here, to determine the contributions of fold versus sequence, the total PB calculated reduction potential for a series of hypothetical solutes was considered, in which each solute becomes progressively more like the final protein model. In each case, the cluster is in the same protein cavity surrounded by water (see Methods), but the cavity is either empty with ε_p = 1 (Fig. 3a), filled with a dielectric of ε_p = 4 referred to as the dielectric-filled cavity (Fig. 3b), filled with a dielectric of ε_p = 4 and backbone charges turned on referred to as the backbone+dielectric cavity (Fig. 3c), or filled with a dielectric of ε_p = 4 and all protein charges turned on (Fig. 3d), which is simply the standard Honig model of the protein.35 The reduction potentials of each of the hypothetical molecules are shown only for the 2-/3- couple (Fig. 4) since the results were essentially the same for the 1-/2- couple except for the scale.

The calculated reduction potentials for the cluster in the empty protein cavities (ε_p = 1) in water (Fig. 3a; Fig. 4, gray) relative to in vacuum indicate that solvating the cavity with water increased the reduction potential by 3 to 5 V, which accounts for 40 to 45% of the total $-\Delta G_{out}/F$. Moreover, the magnitude of the increase was highly dependent on the effective size of the cavity.

The calculated reduction potentials for the cluster in dielectric-filled (ε_p = 4) cavities (Fig. 3b; Fig. 4, red) relative to the empty protein cavities (Fig. 4, gray) indicate that filling the cavity with a dielectric by increasing ε_p from 1 to 4 increased the reduction potential by 1.5 to 3 V, which accounts for another 20 to 25% of the total $-\Delta G_{out}/F$. However, the dependence of the potential on the effective size of the protein decreased as ε_p increased, in agreement with the concentric-sphere model as ε_p increased from 1 to 4, so that the Fds were only ~0.15 V higher than the HiPIPs, and the FePs were only ~0.2 V higher than the Fds.

This implies that filling the cavity with even a relatively low dielectric negated much of the differences between the folds found in solvating the empty cavity.

The calculated reduction potentials of the backbone+dielectric cavities (Fig. 4, blue) relative to the dielectric-filled cavities (Fig. 3c; Fig. 4, red) indicate that the effects of the fold via the arrangement of the backbone increased the reduction potential by another ~0.4 to ~0.9 V, and the positive values of the changes indicate that the backbone in all three proteins was apparently organized to favorably solvate the cluster. The addition of the backbone increased the differences between the folds so that the Fds went from ~0.15 V higher for the dielectric-filled cavities to ~0.4 V higher for the backbone+dielectric cavities than the HiPIPs and the FePs went from ~0.2 V higher for the dielectric-filled cavities to ~0.33 V higher for the backbone+dielectric cavities than the Fds. Moreover, each fold had a different backbone contribution, indicating the backbone contribution was characteristic of the fold.

Finally, the calculated reduction potentials for the entire proteins (Fig. 3d; Fig. 4, yellow) relative to the backbone+dielectric cavities (Fig. 4, blue) indicate that the effects of the sequence via the net contribution of the side chains were smaller than that of the fold since they caused changes of no more than ~0.3 V. Moreover, the contribution of the side chains caused the reduction potentials to vary both above and below the backbone value and they lowered the potential for the Fds and the FePs. Therefore, the potential appeared to be tuned by the side chains, i.e., the sequence, with respect to the relatively constant value set by the backbone, i.e. the fold.

Overall, the solvent made a large contribution to the reduction potential, which was modulated by the proximity of the cluster to the surface of the protein cavity and the difference between the dielectric constant inside and outside the cavity, and the backbone made another large contribution. Moreover, examining the average and standard deviations of the environmental contributions of the dielectric cavities, $-\Delta G\varepsilon_p/F$, and backbone +dielectric cavities, $-\Delta G_{bb}/F$, the contributions of both the location of the cluster in the cavity and the backbone were characteristic for each fold and helped to define differences in the fold contributions; i.e., considering the standard deviations, the values for each fold were distinctly different. Moreover, compared to the total environmental contribution, $-\Delta G_{out}/F$, the average backbone+dielectric contribution was within 0.2 V of the average total contribution while the standard deviations of the dielectric cavity and the backbone +dielectric were much less than the total contribution, indicating that the fold contribution was relatively constant and characteristic of the fold while the side chains tuned the backbone contribution.

Localization of the fold contribution

A relatively local region of the protein may be responsible for most of the fold contribution to potential since it arises from the backbone dipoles and dipolar interactions die off rapidly. To determine which part of the protein is important, the contribution of each peptide group (minus the side chain) was calculated (see methods) as a function of the distance between the center of the C-N peptide bond and the nearest cysteinyl or inorganic sulfur of the redox site were examined for each fold; results for *Tt* HiPIP, *Ca* Fd, and *Av* FeP are shown (Fig. 6) since results for the other proteins with the same folds were similar. The largest contributions were within 5.5 Å of a cluster sulfur, and were both positive and negative in the HiPIPs, only positive in the Fds, and mostly positive in the FePs. In this region, the amide hydrogens point toward the cluster and the carbonyl oxygens point away from the cluster in Fd (Fig. 7b) and Fe protein (Fig. 7c), but are randomly oriented in HiPIP (Fig. 7a).

Since the largest contributions to the potential appear to come from residues close to the cluster (Fig. 6), the solvation free energy was also calculated (see Methods) for hypothetical

solutes that had only backbone peptide groups outside or inside of a cutoff, $-\Delta G_{bb(out)}/F$ (Fig. 5, pink) or $-\Delta G_{bb(in)}/F$, (light blue), respectively, but with a dielectric filled protein cavity determined by the entire protein (Fig. 5, red column). For a cutoff of 5.5 Å, $-\Delta G_{bb(out)}/F$ was generally close to $-\Delta G\varepsilon_p/F$, implying that the outer part of the backbone does not significantly contribute to the solvation free energy, while $-\Delta G_{bb(in)}/F$ was generally close to $-\Delta G_{bb}/F$ (Fig. 5, dark. blue column), implying that just the inner part of the backbone gives rise to most of the backbone contribution. Since the cysteinyl sulfurs and inorganic sulfurs are 3.9 and 2.2 Å from the cluster center, respectively, most of the backbone contribution apparently came from residues within ~10 Å of the cluster center.

However, although most of the backbone contribution appeared to be very local, the region outside is still important because it defines the low dielectric cavity of the entire protein. For example, although the close values of $-\Delta G_{bb(in)}/F$ and $-\Delta G_{bb}/F$ simply implies that the peptide partial charges beyond 5.5 Å from redox site sulfurs did not contribute much, the solvation energy of a fragment consisting of the inner residues with a low dielectric cavity defined only by these residues is much larger. Thus, although the location of the cluster relative to the cavity surface is important, the size of the low dielectric cavity cannot be ignored. Moreover, contributions of the polypeptide can extend beyond 5.5 Å. For example, the Fe protein is much larger than the HiPIPs or Fds and so the number density of peptide groups as a function of peptide-sulfur distance (Fig. 6) is large well past 15 Å for the FePs unlike the other two. For a cutoff of 5.5 Å in FeP, $-\Delta G_{bb(out)}/F$ was slightly higher than $-\Delta G_{\varepsilon p}/F$ and $-\Delta G_{bb(in)}/F$ was slightly lower than $-\Delta G_{bb}/F$ so that the residues within 5.5 Å of redox site sulfurs accounted for ~75% of the backbone contribution. However, for a cutoff of 15.5 Å, $-\Delta G_{bb(out)}/_F$ was essentially equal to $-\Delta G_{\varepsilon p}/F$ and $-\Delta G_{bb(in)}/F$ was essentially equal to $-\Delta G_{bb}/F$ so that the remaining 25% of the backbone contribution came mainly from many small contributions between 5.5 and 15.5 Å of a redox site sulfur, or ~10 to ~20Å of the cluster center (Fig. 6).

Conclusions

The protein environment plays an important role in protein-mediated electron transfer in part by poising poises the reduction potentials of the redox sites at specific values. Moreover, mutational studies of the reduction potential are an exquisite experimental probe of the local electrostatic environment, which also can be important in the catalytic activity of enzymes. The combined results of the DFT calculations of the intrinsic contribution and the PB calculations of the environmental contribution reproduce the experimental reduction potentials remarkably well. Using structures from multiple homologous proteins in three different folds, we examined consistencies within a fold and differences between folds to separate the contributions of fold versus sequence.

The results here indicate that the fold plays the major role in determining the reduction potential while the side chains tune the reduction potential, here by less than ~0.3 V with respect to the backbone. In addition, while the fold could potentially affect the reduction potential by the size and shape of the cavity, the cluster location within the cavity, and the arrangement of the backbone partial charges around the cluster, the results here indicate that the proximity of cluster to the cavity surface is more important than the size of the protein. Also, the results indicate that the extent of polarization for the backbone around the cluster is important, especially within ~10 Å of the cluster center. Moreover, in examining six HiPIPs, four Fds, and four FeP or FeP related proteins, the results were consistent within a fold but differed between the folds, particularly when only the cavity and/or the backbone contributions were considered. Thus, the contributions the backbone were characteristic for each fold and helped to define differences in the fold contributions while the side chains

mainly tuned the backbone contribution and were responsible for greater variation within a fold.

More generally, the results here indicate that the local environment plays the largest role in determining the redox potentials, since the potential is raised by oriented polar groups to the cluster, whether from the solvent or the protein. Thus, reduction potentials for proteins with the same environment for the cluster (i.e. similar binding motif) should have similar reduction potentials whether the motif is found in a small aqueous protein or in a large protein complex, with or without a bound redox partner, as long as the cluster does not become more or less buried. Thus, binding far from the cluster will have little effect. However, for a cluster close to the surface, binding across the most solvent exposed face (as is often the case for a redox partner) may lower the reduction potential unless the partner is also polarized in the same direction as the solvent it replaces with respect to the cluster.

Supplementary Material

Refer to Web version on PubMed Central for supplementary material.

Acknowledgments

This work was supported by a grant from the National Institutes of Health (GM-45303). The views and conclusions contained in this document are those of the author and should not be interpreted as necessarily representing the official policies or endorsements, either expressed or implied, of the U. S. Government. Support from the William G. McGowan Foundation is also gratefully acknowledged. We also thank Sergio A. Hassan, Angela Gronenborn, and Douglas C. Rees for helpful discussions. In addition, this research was supported in part by the Intramural Research Program of the NIH, National Heart, Lung, and Blood Institute (Laboratory of Computational Biology).

References

1. Lippard, SJ.; Berg, JM. Principles of Bioinorganic Chemistry. Mill Valley, CA: University Science Books; 1994.
2. Page CC, Moser CC, Dutton PL. Mechanism for electron transfer within and between proteins. Curr Opin Chem Biol. 2003; 7:551–556. [PubMed: 14580557]
3. Winker, JR.; Gray, HB.; Prytkova, TR.; Kurnikov, IV.; Beratan, DN. Electron transfer through proteins. In: Willner, I.; Katz, E., editors. Bioelectronics: From Theory to Applications. Weinheim, Germany: Wiley-VCH; 2005. p. 15-33.
4. Ichiye, T. Computational Studies of Redox Potentials of Electron Transfer Proteins. In: Pratt, LR.; Hummer, G., editors. Simulation and Theory of Electrostatic Interactions in Solution. Sante Fe, New Mexico: American Institute of Physics; 1999. p. 431-450.
5. Jensen GM, Warshel A, Stephens PJ. Calculation of the Redox Potentials of Iron-Sulfur Proteins: The 2-/3- Couple of $[Fe_4S_4^*Cys_4]$ Clusters in *Peptococcus aerogenes* Ferredoxin, *Azotobacter vinelandii* Ferredoxin I, and *Chromatium vinosum* High-Potential Iron Protein. Biochem. 1994; 33:10911–10924. [PubMed: 8086408]
6. Rees DC. Electrostatic influence on energetics of electron transfer reactions. Proc Natl Acad Sci USA. 1985; 82(10):3082–3085. [PubMed: 3858805]
7. Ichiye, T. Simulations of electron transfer proteins. In: Becker, OM.; MacKerell, AD., Jr; Roux, B.; Watanabe, M., editors. Computational Biochemistry and Biophysics. New York, NY: Marcer Dekker, Inc; 2001. p. 393-415.
8. Reiss H, Heller A. The absolute potential of the standard hydrogen electrode: a new estimate. J Phys Chem. 1985; 89(20):4207–4213.
9. Venkateswara RP, Holm RH. Synthetic analogues of the active sites of iron-sulfur proteins. Chem Rev. 2004; 104(2):527–559. [PubMed: 14871134]
10. Hall DO, Cammack R, Rao KK. Role for the ferredoxins in the origin of life and biological evolution. Nature. 1971; 223:136–138. [PubMed: 12058758]

11. Beinert H. Iron-sulfur proteins: Ancient structures, still full of surprises. J Biol Inorg Chem. 2000; 5:2–15. [PubMed: 10766431]
12. Watt GD, Reddy KRN. Formation of an all Ferrous Fe_4S_4 Cluster in the Iron Protein Component of *Azotobacter vinelandii* Nitrogenase. J Inorg Biochem. 1994; 53:281–294.
13. Torres RA, Lovell T, Noodleman L, Case DA. Density Functional and Reduction Potential Calculations of Fe_4S_4 Clusters. J Am Chem Soc. 2003; 125:1923–1936. [PubMed: 12580620]
14. Stephens P, Jollie D, Warshel A. Protein Control of Redox Potentials of Iron- Sulfur Proteins. Chem Rev. 1996; 96:2491–2514. [PubMed: 11848834]
15. Dey A, Jenney FE Jr, Adams MWW, Babini E, Takahara Y, Fukuyama K, Hodgson KO, Hedman B, Solomon EI. Solvent Tuning of Electrochemical Potentials in the Active Sites of HiPIP Versus Ferredoxin. Science. 2007; 318:1464–1468. [PubMed: 18048692]
16. Langen R, Jensen GM, Jacob U, Stephens PJ, Warshel A. Protein Control of Iron-Sulfur Cluster Redox Potentials. J Biol Chem. 1992; 267(36):25625–25627. [PubMed: 1464583]
17. Swartz PD, Beck BW, Ichiye T. Structural Origins of Redox Potentials in Fe-S Proteins: Electrostatic Potentials of Crystal Structures. Biophys J. 1996; 71:2958–2969. [PubMed: 8968568]
18. Eidsness MK, Burden AE, Richie KA, Kurtz DMJ, Scott RA, Smith ET, Ichiye T, Beard B, Min T, Kang C. Modulation of the Redox Potential of the [Fe(SCys)4] Site in Rubredoxin by the Orientation of a Peptide Dipole. Biochemistry. 1999; 38:14803–14809. [PubMed: 10555962]
19. Beck BW, Xie Q, Ichiye T. Sequence Determination of Reduction Potentials by Cysteinyl Hydrogen Bonds and Peptide Dipoles in [4Fe-4S] Ferredoxins. Biophys J. 2001; 81:601–613. [PubMed: 11463610]
20. Yelle RB, Park N-S, Ichiye T. Molecular dynamics simulations of rubredoxin from *Clostridium pasteurianum:* Changes in structure and electrostatic potential during redox reactions. Proteins: Structure, Function, and Genetics. 1995; 22:154–167.
21. Swartz P, Ichiye T. Temperature dependence of the redox potential of rubredoxin from *Pyrococcus furiosus:* A molecular dynamics study. Biochemistry. 1996; 35:13772–13779. [PubMed: 8901519]
22. Min T, Ergenekan CE, Eidsness MK, Ichiye T, Kang C. Leucine 41 is a gate for water entry in the reduction of Clostridium pasteurianum rubredoxin. Protein Science: A Publication of the Protein Society. 2001; 10:613. [PubMed: 11344329]
23. Langen R, Jensen G, Jacob U, Stephens P, Warshel A. Protein control of iron-sulfur cluster redox potentials. Journal of Biological Chemistry. 1992; 267:25625–25627. [PubMed: 1464583]
24. Jensen GM, Warshel A. Calculation of the Redox Potentials of Iron-Sulfur Proteins: The 2-/3- Couple of [Fe4S4Cys4] Clusters in Peptococcus aerogenes Ferredoxin Azotobacter vinelandii Ferredoxin I, and Chromatium vinosum High-Potential Iron Protein. Biochemistry. 1994; 33:10911–10924. [PubMed: 8086408]
25. Mouesca J-M, Chen JL, Noodleman L, Bashford D, Case DA. Density Functional/Poisson-Boltzmann Calculations of Redox Potentials for Iron-Sulfur Clusters. J Am Chem Soc. 1994; 116:11898–11914.
26. Noodleman L, Peng CY, Case DA, Mouesca JM. Orbital interactions, electron delocalization and spin coupling in iron-sulfur clusters. Coord Chem Rev. 1995; 144:199–241.
27. Yang X, Niu S, Ichiye T, Wang LS. Direct Measurement of the Hydrogen-Bonding Effect on the Intinsic Redox Potentials of [4Fe-4S] Cubane Complexes. J Am Chem Soc. 2004; 126:15790–15794. [PubMed: 15571403]
28. Niu S, Ichiye T. Insight into environmental effects on bonding and redox properties of [4Fe-4S] clusters in proteins. J Am Chem Soc. 2009; 131(16):5724–5725. [PubMed: 19341280]
29. Parr, RG.; Yang, W. Density-Functional Theory of Atoms and Molecules. Oxford: Oxford University Press; 1989.
30. Niu S, Wang XB, Nichols JA, Wang LS, Ichiye T. Combined Quantum Chemistry and Photoelectron Spectroscopy Study of the Electronic Structure and Reduction Potentials of Rubredoxin Redox Site Analogues. J Phys Chem A. 2003; 107:2898–2907.
31. Fu YJ, Niu S, Ichiye T, Wang LS. Electronic Structure and Intrinsic Redox Properties of [2Fe-2S] $^{+}$Clusters with Tri- and Tetracoordinated Iron Sites. Inorg Chem. 2005; 44:1202–1204. [PubMed: 15732958]

32. Wang X-B, Niu S, Yang X, Ibrahim SK, Pickett CJ, Ichiye T, Wang L-S. Probing the Intrinsic Electronic Structure of the Cubane [4Fe-4S] Cluster: Nature's Favorite Cluster for Electron Transfer and Storage. J Am Chem Soc. 2003; 125:14072–14081. [PubMed: 14611244]
33. Niu S, Nichols JA, Ichiye T. Optimization of Spin-Unrestricted Density Functional Theory for Redox Properties of Rubredoxin Redox Site Analogues. J Chem Theory Comput. 2009; 5(5): 1361–1368. [PubMed: 20161267]
34. Honig B, Nicholls A. Classical Electrostatics in Biology and Chemistry. Science. 1995; 268 114–1149.
35. Gilson MK, Sharp KA, Honig BH. Calculating the electrostatic potential of molecules in solution: Method and error assessment. J Comput Chem. 1988; 9(4):327–335.
36. Swartz P, Beck B, Ichiye T. Structural origins of redox potentials in Fe-S proteins electrostatic potentials of crystal structures. Biophysical journal. 1996; 71:2958–2969. [PubMed: 8968568]
37. Berman HM, Westbrook J, Feng Z, Gilliland G, Bhat TN, Weissig H, Shindyalov IN, Bourne PE. The Protein Data Bank. Nucleic Acids Res. 2000; 28:235–242. [PubMed: 10592235]
38. Rayment I, Wesenberg G, Meyer TE, Cusanovich MA, Holden HM. Three-dimensional structure of the high-potential iron-sulfur protein isolated from the purple phototrophic bacterium *Rhodocyclus tenuis* determined and refined at 1.5 Å resolution. J Mol Biol. 1992; 228:672–686. [PubMed: 1453470]
39. Gonzalez A, Benini S, Ciurli S. Structure of *Rhodoferax fermentans* high-potential iron-sulfur protein solved by MAD. Acta Crystallogr. 2003; D59:1582–1588.
40. Benning MM, Meyer TE, Rayment I, Holden HM. Molecular Structure of the Oxidized High-Potential Iron-Sulfur Protein Isolated from *Ectothiorhodospira vacuolata*. Biochem. 1994; 33:2476–2483. [PubMed: 8117708]
41. Breiter DR, Meyer TE, Rayment I, Holden HM. The Molecular Structure of the High Potential Iron-Sulfur Protein Isolated from *Ectothiorhodospira halophila* Determined at 2.5-Å Resolution. J Biol Chem. 1991; 266(28):18660–18667. [PubMed: 1917989]
42. Liu L, Nogi T, Kobayashi M, Nozawa T, Miki K. Ultrahigh-resolution structure of high-potential iron-sulfur protein from *Thermochromatium tepidum*. Acta Crystallogr. 2002; D58:1085–1091.
43. Parisini E, Capozzi F, Lubini P, Lamzin V, Luchinat C, Sheldrick GM. *Ab initio* solution and refinement of two high-potential iron protein structures at atomic resolution. Acta Crystallogr. 1999; D55:1773–1784.
44. Dauter Z, Wilson KS, Sieker LC, Meyer J, Moulis JM. Atomic resolution (0.94 Å) structure of *Clostridium acidurici* ferredoxin. Detailed geometry of [4Fe-4S] clusters in a protein. Biochem. 1997; 36:16065–16073. [PubMed: 9405040]
45. Backes G, Mino Y, Loehr TM, Meyer TE, Cusanovich M, Sweeney WV, Adman ET, Sanders-Loehr J. The Environment of Fe_4S_4 Clusters in Ferredoxins and High-Potential Iron Proteins. New Information from X-ray Crystallography and Resonance Raman Spectroscopy. J Am Chem Soc. 1991; 113:2055–2064.
46. Giastas P, Pinotsis N, Efthymiou G, Wilmanns M, Kyritsis P, Moulis J-M, Mavridis IM. The structure of the 2[4Fe-4S] ferredoxin from *Pseudomonas aeruginosa* at 1.32-Å resolution: comparison with other high-resolution structures of ferredoxins and contributing structural features to reduction potential values. J Biol Inorg Chem. 2006; 11:445–458. [PubMed: 16596388]
47. Moulis JM, Sieker LC, Wilson KS, Dauter Z. Crystal structure of the 2[4Fe-4S] ferredoxin from *Chromatium vinosum*: evolutionary and mechanistic inferences for [3/4Fe-4S] ferredoxins. Protein Science. 1996; 5:1765–1775. [PubMed: 8880900]
48. Jang SB, Seefeldt LC, Peters JW. Insights into Nucleotide Signal Transduction in Nitrogenase: Structure of an Iron Protein with MgADP Bound. Biochem. 2000; 39:14745–14752. [PubMed: 11101289]
49. Schlessman JL, Woo D, Joshua-Tor L, Howard JB, Rees DC. Conformational Variability in the Structures of the Nitrogenase Iron Proteins from *Azotobacter vinelandii* and *Clostridium pasteurianum*. J Mol Biol. 1998; 280:669–685. [PubMed: 9677296]
50. Strop P, Takahara PM, Chiu H-J, Angove HC, Burgess BK, Rees DC. Crystal Structure of the All-Ferrous $[4Fe\text{-}4S]^0$ Form of the Nitrogenase Iron Protein from *Azotobacter vinelandii*. Biochem. 2001; 40:651–656. [PubMed: 11170381]

51. Sarma R, Barney BM, Hamilton TL, Jones A, Seefeldt LC, Peters JW. Crystal structure of the L protein of *Rhodobacter sphaeroides* light-independent protochlorophyllide reductase with MgADP Bound: A homologue of the nitrogenase Fe protein. Biochem. 2008; 47:13004–13015. [PubMed: 19006326]
52. Hagen KS, Watson AD, Holm RH. Analogs of the $[Fe_4S_4]^+$ sites of reduced ferredoxins: single-step synthesis of the clusters $[Fe_4S_4(SR)_4]^{3-}$ and examples of compressed tetragonal core structures. Inorg Chem. 1984; 23:2984–2990.
53. Heering HA, Bulsink YBM, Hagen WR, Mayer TE. Influence of Charge and Polarity on the Redox Potentials of High-Potential Iron-Sulfur Proteins: Evidence for the Existence of Two Groups. Biochem. 1995; 34:14675–14686. [PubMed: 7578075]
54. Hochkoeppler A, Ciurli S, Venturoli G, Zannoni D. The high potential iron-sulfur protein (HiPIP) from *Rhodoferax fermentans* is competent in photosynthetic electron transfer. FEBS Lett. 1995; 357:70–74. [PubMed: 8001683]
55. Heering HA, Bulsink YBM, Hagen WR, Meyer TE. Reversible super-reduction of the cubane $[4Fe\text{-}4S]^{(3+;2+;1+)}$ in the high-potential iron-sulfur protein under non-denaturing conditions. Eur J Biochem. 1995; 232:811–817. [PubMed: 7588720]
56. Armstrong FA, Hill HAO, Walton NJ. Direct electrochemical oxidation of *Clostridium pasteurianum* ferredoxin. FEBS Lett. 1982; 150(1):214–218.
57. Kyritsis P, Hatzfeld OM, Link TA, Moulis J-M. The Two [4Fe-4S] Clusters in *Chromatium vinosum* Ferredoxin Have Largely Different Reduction Potentials. J Biol Chem. 1998; 273(25): 15404–15411. [PubMed: 9624123]
58. Stombaugh NA, Sundquist JE, Burris RH, Orme-Johnson WH. Oxidation-reduction properties of several low potential iron-sulfur proteins and of methylviologen. Biochem. 1976; 15(12):2633–2641. [PubMed: 181047]
59. Watt GD, Wang Z-C, Knotts RR. Redox reactions of and nucleotide binding to the iron protein of *Azotobacter vinelandii*. Biochem. 1986; 25(25):8156–8162.
60. Chan JM, Ryle MJ, Seefeldt LC. Evidence that MgATP accelerates primary electron transfer in a *Clostridium pasteurianum* Fe Protein-*Azotobacter vinelandii* MoFe Protein Nitrogenase Tight Complex. J Biol Chem. 1999; 274(25):17593–17598. [PubMed: 10364195]
61. Group HPCC. NWChem, A Computational Chemistry Package for Parallel Computers, Version 4.5. Richland, WA 99352: Pacific Northwest National Laboratory; 2003.
62. Baker NA, Sept D, Joseph S, Holst MJ, McCammon JA. Electrostatics of nanosystems: application to microtubules and the ribosome. Proc Natl Acad Sci USA. 2001; 98:10037–10041. [PubMed: 11517324]
63. Perrin BS Jr, Ichiye T. Accurate Calculation for FeS Reduction Potentials. To Be Published. 2009
64. Brooks BR, Bruccoleri RE, Olafson BD, States DJ, Swaminathan S, Karplus M. CHARMM: A Program for Macromolecular Energy, Minimization, and Dynamics Calculations. J Comp Chem. 1983; 4:187–217.
65. Connolly ML. Solvent-accessible surfaces of proteins and nucleic-acids. Science. 1983; 221:709–713. [PubMed: 6879170]
66. Bruccoleri RE, Novotny JR, Davis ME, Sharp K. Finite Difference Poisson-Boltzmann Electrostatic Calculations: Increased Accuracy Achieved by Harmonic Dielectric Smoothing and Charge Antialiasing. J Comput Chem. 1997; 18(2):268–276.
67. Warshel A, Sharma KD, Kato M, Parson WW. Modeling electrostatic effects in proteins. Biochim Biophys Acta. 2006; 1764:1647–1676. [PubMed: 17049320]

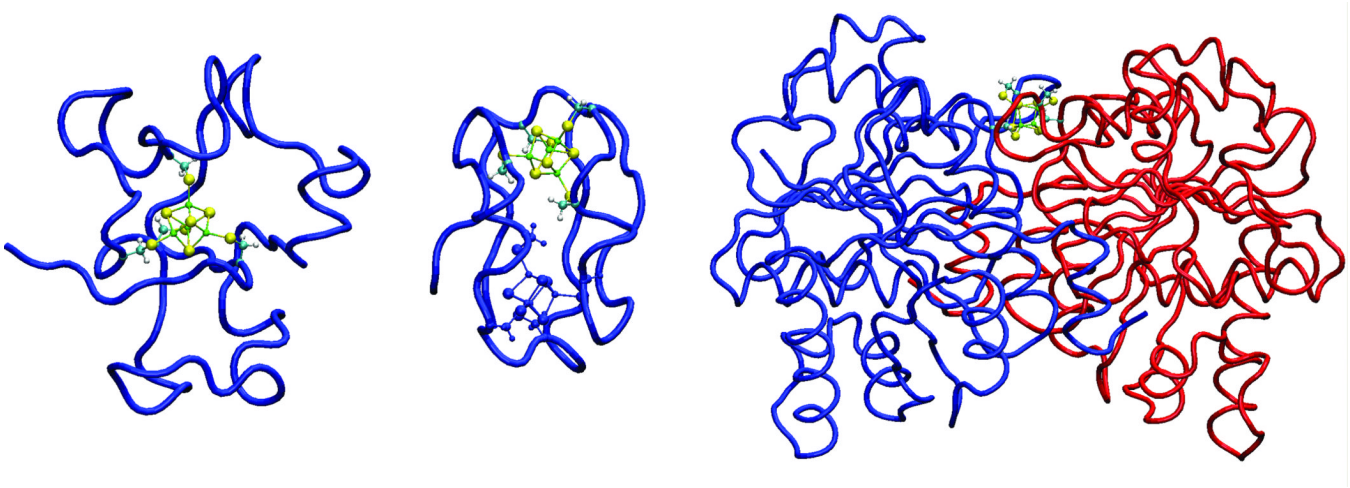

Figure 1.

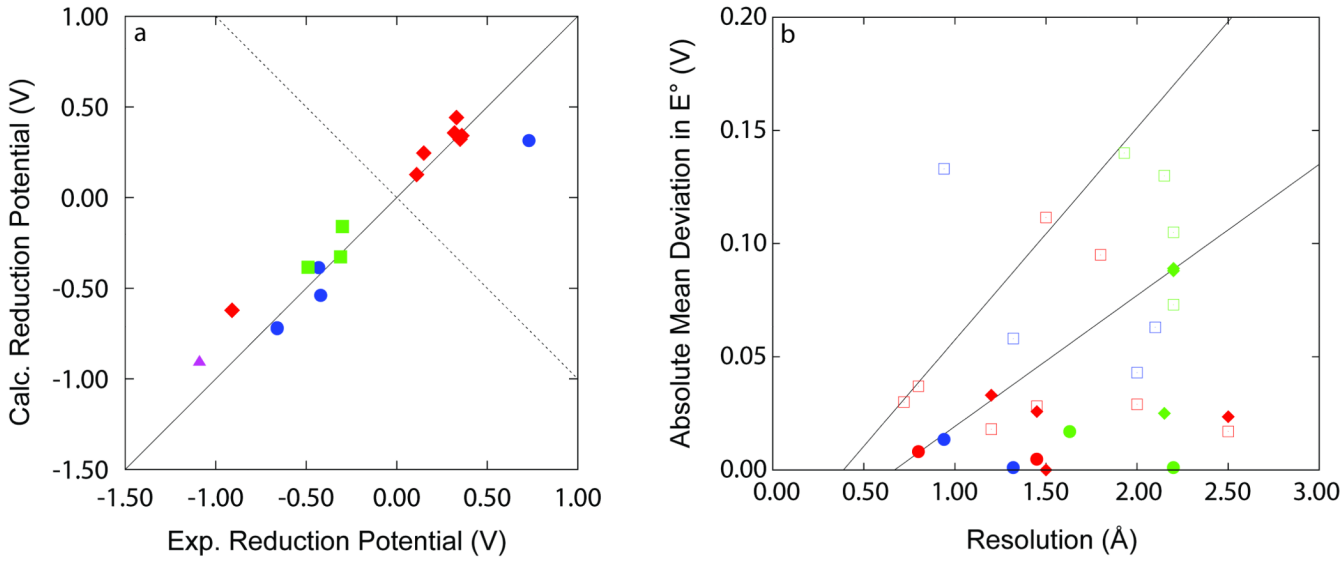

Figure 2.

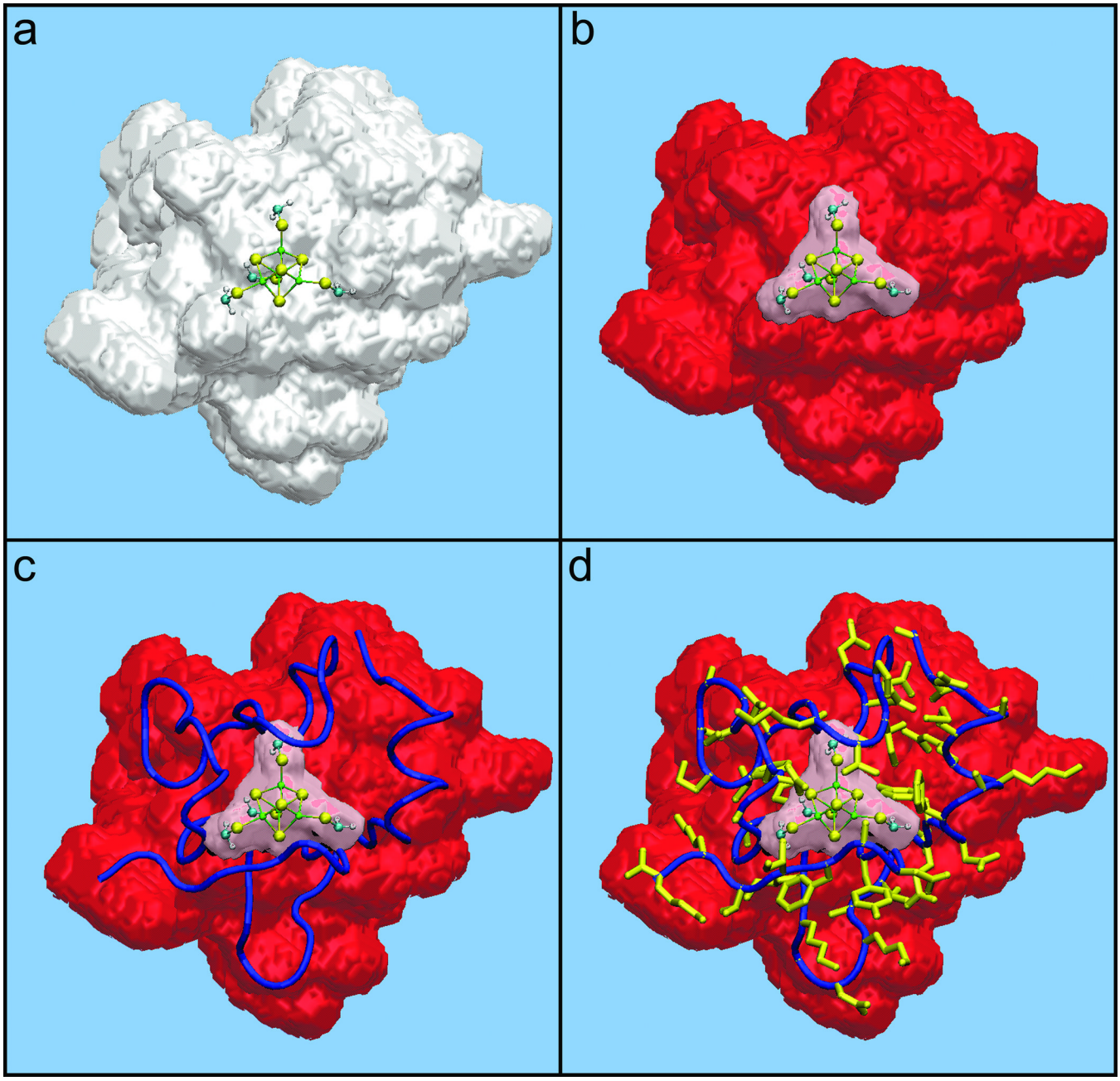

Figure 3.

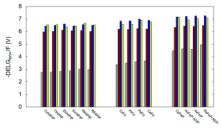

Figure 4.

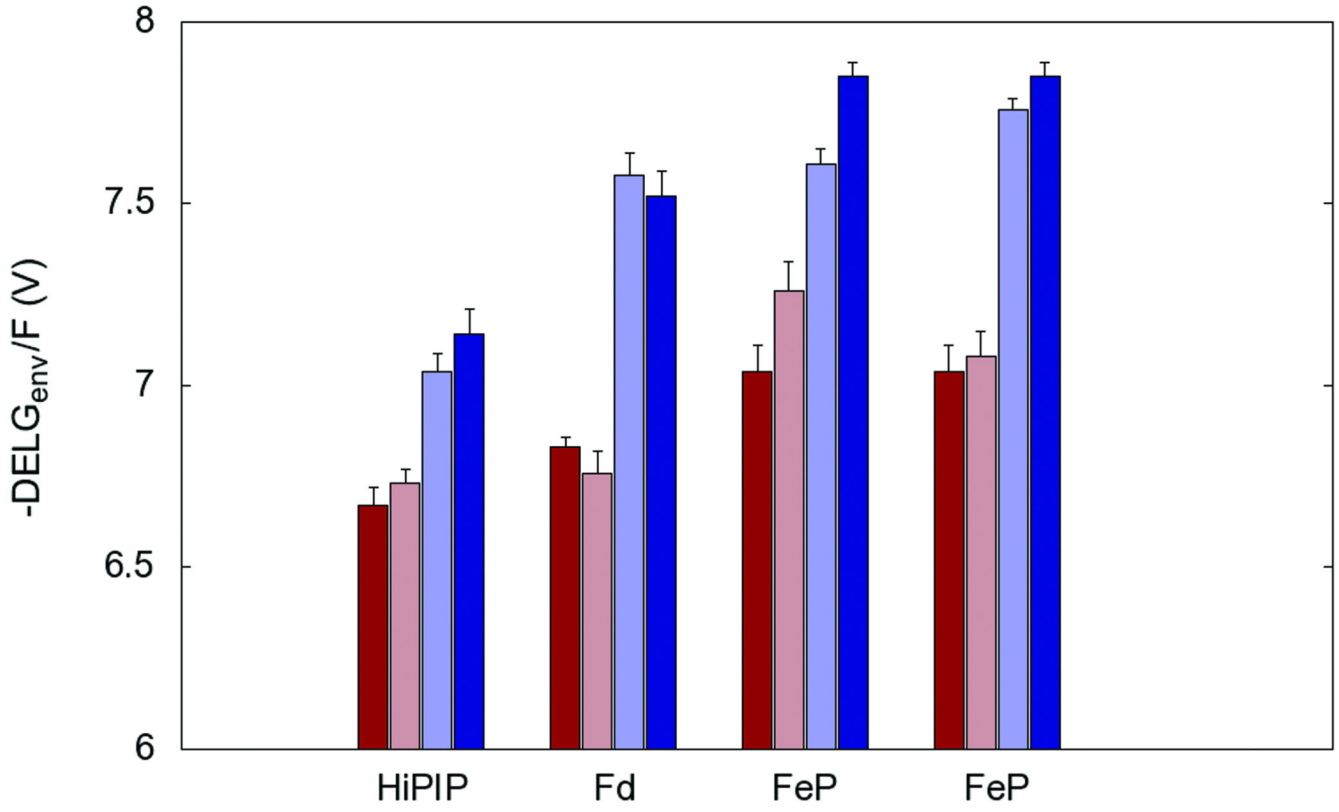

Figure 5.

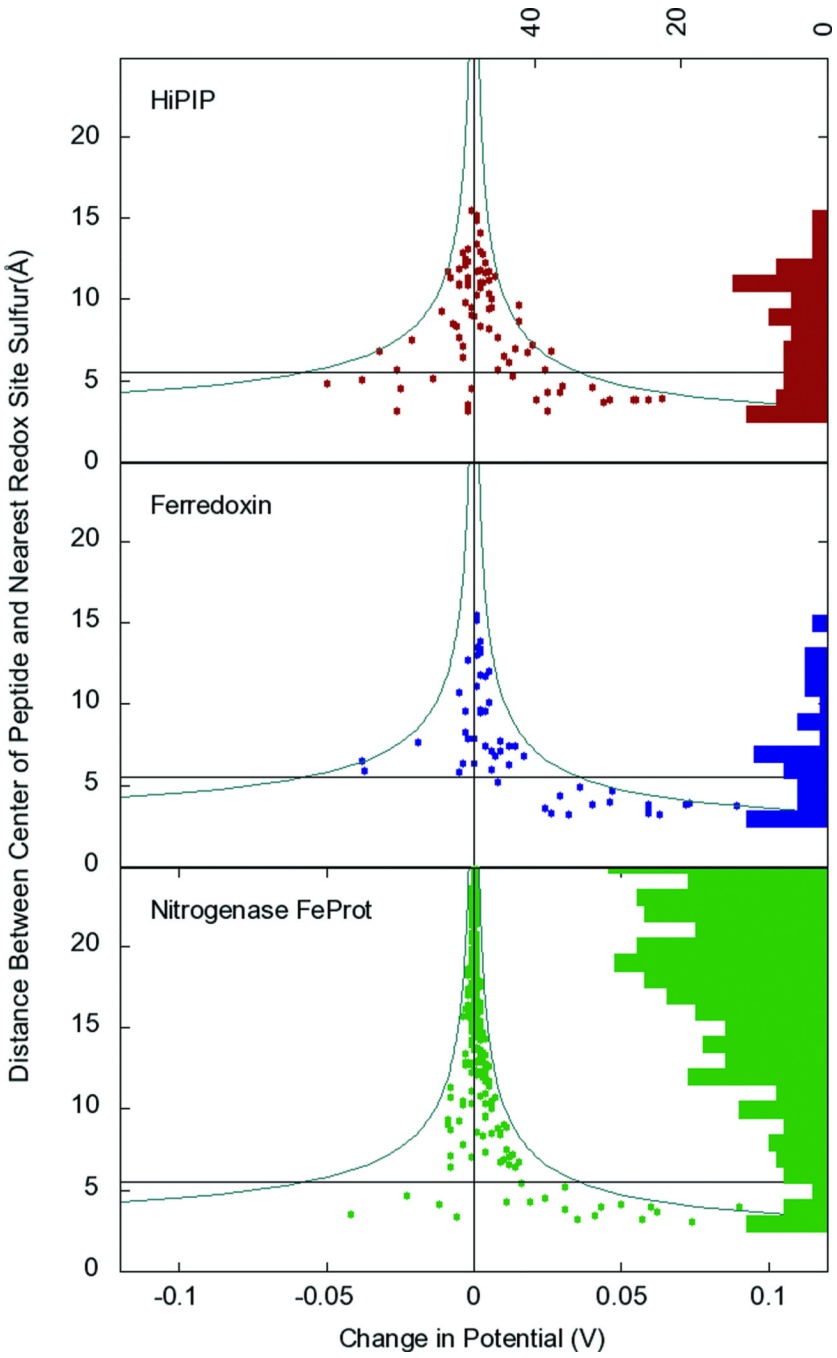

Figure 6.

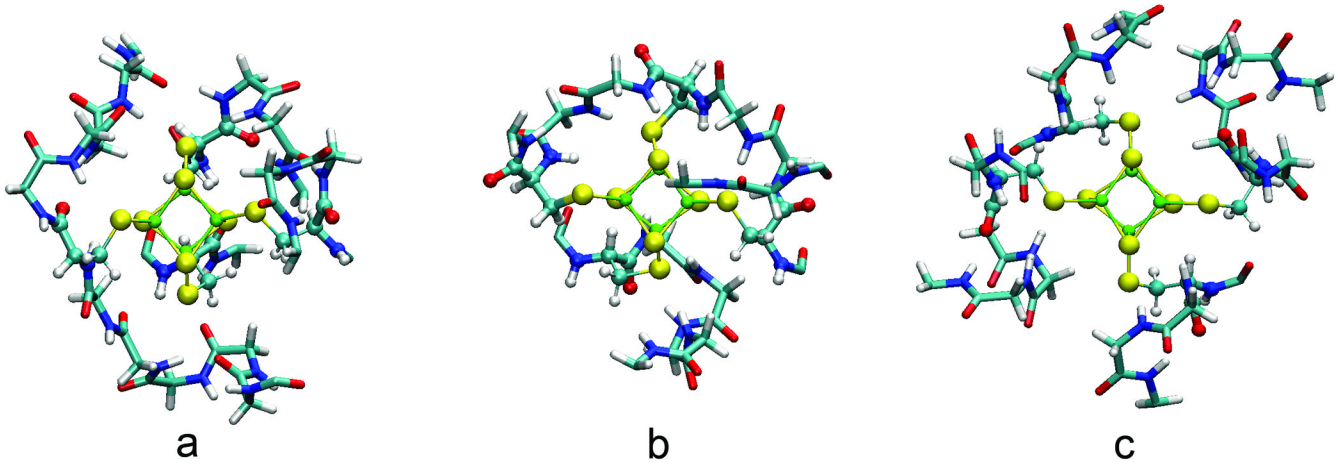

Figure 7.

Table I

Intrinsic and environmental contributions ($-\Delta G_{in}/F$ and $-\Delta G_{out}/F$, respectively) to the calculated reduction potentials, and calculated and experimental reduction potentials ($E°$) vs. SHE for different proteins, all in V. Superscripts on proteins indicate couple of the redox site.

Protein	$-\Delta G_{in}/F$	$-\Delta G_{out}/F$	Calc. $E°$	Exp. $E°$*
$HiPIP^{1-/2-}$	0.26	4.43 ± 0.11	0.31 ± 0.11	0.27 ± 0.11
$Fd^{1-/2-}$	0.26	4.62 ± 0.15	0.44 ± 0.15	0.73
$FeP^{1-/2-}$	0.26	4.83 ± 0.10	0.66 ± 0.10	>>0
$HiPIP^{2-/3-}$	−3.48	7.13 ± 0.10	−0.78 ± 0.10	−0.91
$Fd^{2-/3-}$	−3.48	7.32 ± 0.16	−0.59 ± 0.16	−0.54 ± 0.15
$FeP^{2-/3-}$	−3.48	7.64 ± 0.06	−0.28 ± 0.08	−0.35 ± 0.09

[a] For references for experimental values, see methods. The reduction potential for $FeP^{1-/2-}$ was assumed from $FeP^{2-/3-}$ measured potentials.